



HAL
open science

Enhancing interface stability and ionic conductivity in the designed $\text{Na}_3\text{SbP}_{0.4x}\text{S}_{4-x}\text{O}_x$ sulfide solid electrolyte through bridging oxygen

Lingjun Shu, Chengwei Gao, Yongxing Liu, Xiaolong Zhou, Hongli Ma, Xianghua Zhang, Xiang Shen, Shixun Dai, Changgui Lin, Qing Jiao

► To cite this version:

Lingjun Shu, Chengwei Gao, Yongxing Liu, Xiaolong Zhou, Hongli Ma, et al.. Enhancing interface stability and ionic conductivity in the designed $\text{Na}_3\text{SbP}_{0.4x}\text{S}_{4-x}\text{O}_x$ sulfide solid electrolyte through bridging oxygen. *Journal of Colloid and Interface Science*, 2023, 652 (Part B), pp.2042-2053. 10.1016/j.jcis.2023.09.013 . hal-04226695

HAL Id: hal-04226695

<https://hal.science/hal-04226695>

Submitted on 31 Oct 2023

HAL is a multi-disciplinary open access archive for the deposit and dissemination of scientific research documents, whether they are published or not. The documents may come from teaching and research institutions in France or abroad, or from public or private research centers.

L'archive ouverte pluridisciplinaire **HAL**, est destinée au dépôt et à la diffusion de documents scientifiques de niveau recherche, publiés ou non, émanant des établissements d'enseignement et de recherche français ou étrangers, des laboratoires publics ou privés.



Distributed under a Creative Commons Attribution - NonCommercial 4.0 International License

Enhancing interface stability and ionic conductivity in the designed $\text{Na}_3\text{SbP}_{0.4x}\text{S}_{4-x}\text{O}_x$ sulfide solid electrolyte through bridging oxygen

Lingjun Shu^{a, b}, Chengwei Gao^{a, b}, Yongxing Liu^{a, c}, Xiaolong Zhou^d, Hongli Ma^e, Xianghua Zhang^e, Xiang Shen^{a, b, c, f}, Shixun Dai^a, Changgui Lin^{a*, c}, and Qing Jiao^{a, c*}

^a Laboratory of Infrared Material and Devices, Advanced Technology Research Institute, Ningbo University, Ningbo 315211, China

^b Faculty of Information Science and Engineering, Ningbo University, Ningbo 315211, China

^c Engineering Research Center for Advanced Infrared Photoelectric Materials and Devices of Zhejiang Province, Ningbo 315211, China

^d Faculty of Materials Science and Engineering, Kunming University of Science and Technology, Kunming, 650093

^e Laboratory of Glasses and Ceramics, Institute of Chemical Science, University of Rennes 1, UMR CNRS 6226, Rennes, France

^f Ningbo Institute of Oceanography, Ningbo 315832, China

ABSTRACT

The all-solid-state sodium battery has emerged as a promising candidate for energy storage. However, the limited electrochemical stability of the solid electrolyte, particularly in the presence of Na metal at the anode, along with low ionic conductivity, hinders its widespread application. In this work, the design of P and O elements in Na_3SbS_4 solid electrolyte was investigated through a series of structural tests and characterizations. The electrochemical stability was remarkably improved in the $\text{Na}/\text{Na}_3\text{SbP}_{0.16}\text{S}_{3.6}\text{O}_{0.4}/\text{Na}$ battery, exhibiting a stability of 260 h under a current of 0.1 mA cm^{-2} . Additionally, the room temperature conductivity of $\text{Na}_3\text{SbP}_{0.16}\text{S}_{3.6}\text{O}_{0.4}$ was enhanced to 3.82 mS cm^{-1} , maintaining a value comparable to commercial standards. The proposed design strategy provides an approach for developing sodium ion solid-state batteries with high energy density and long lifespan. The stability of the solid electrolyte interface at the Na | solid electrolyte interface proves critical for the successful assembly of all-solid-state sodium ion batteries.

Keywords: Sulfide solid electrolyte; Sodium ions conductor; Aliovalent substitution; Conductivity.

1. Introduction

The rapid development of portable electronic devices, electric vehicles, and stationary energy storage emphasizes the critical requirement for lithium-ion batteries to exhibit high safety and high energy density[1]. However, lithium-ion batteries face limitations in supporting the scale development of new energy industries due to the depletion of global lithium resources[2]. Moreover, traditional lithium-ion batteries utilizing liquid organic electrolytes present safety concerns, such as thermal runaway caused by overcharging, fire hazards, and short circuits, necessitating the development of new electrolyte materials[3].

Solid-state sodium ion batteries, employing a solid-state electrolyte, offer a solution by effectively mitigating issues related to electrolyte leakage and thermal runaway. The abundance and accessibility of sodium resources make sodium ion batteries particularly appealing compared with lithium-ion batteries[4]. Thus, sodium ion solid-state batteries have gained traction and witness rapid development in applications with lower energy density requirements, including grid energy storage, low-speed electric vehicles, and home energy storage, as a response to increasing lithium prices and resource scarcity[5].

Solid-state electrolytes, crucial materials for solid-state batteries, are broadly classified into three categories: polymeric solid electrolytes, inorganic solid electrolytes, and mixtures of the two. However, the widespread use of polymer electrolytes has been severely limited by issues, such as low ionic conductivity, inadequate electrochemical stability, and poor flame retardancy at ambient temperature, despite their advantages in mechanical flexibility and close electrode contact[6]. By contrast, inorganic compound materials, such as sulfide electrolytes and oxide-based electrolytes, exhibit remarkably higher ionic conductivity compared with polymer electrolytes, often exceeding 10^{-3} S cm^{-1} at ambient temperature[7]. This characteristic makes them excellent candidates for solid-state electrolytes. However, despite the ultrahigh ionic conductivity of sulfide electrolytes, challenges related to stability (both electrochemical stability and interface stability) still need to be addressed. Furthermore, , the solid electrolyte must be able to

withstand Na-mediated direct chemical and electrochemical interactions to prevent sodium dendrites from penetrating the solid electrolyte during battery assembly[8]. Thus, the new solid electrolytes for all-solid-state sodium batteries must possess excellent ion transport characteristics and meet stringent requirements for chemical stability. Currently, the most commonly used sodium ion superconductor electrolyte is based on the Na_3SbS_4 system, which exhibits conductivity of up to $10^{-3} \text{ S cm}^{-1}$. However, its electrochemical stability falls short of expectations. In 2020, Michael Lazar et al. reported the stabilization of sodium metal by using the solid electrolyte Na_3PS_4 (NPS) and its oxygen-doped derivative $\text{Na}_3\text{PS}_{4-x}\text{O}_x$ (NPSO)[9], demonstrating the effectiveness of O doping on Na_3PS_4 . This was attributed to the formation of Na_2O insulation components at the Na/solid electrolyte interface. In 2022, further research demonstrated that introducing O into Na_3PS_4 resulted in electrochemically stable solid-state electrolytes. Additionally, P_2S_5 was identified as a potent glass-forming agent, crucial for inhibiting the propagation of Na dendrites[10]. Furthermore, the addition of oxygen elements induced the formation of structurally enhanced bridging oxygen. However, the ion conductivity of the Na_3PS_4 -based electrolyte system remains limited to 0.27 mS cm^{-1} , falling short of the requirements for solid-state batteries. Moreover, whether the concept of creating solid electrolytes with stable electrochemical performance through the incorporation of P and O elements can be applied to Na_3SbS_4 with fast ion conduction capabilities remains to be determined.

In this work, we synthesized the solid-state electrolyte $\text{Na}_3\text{SbP}_{0.4x}\text{S}_{4-x}\text{O}_x$ (NaSbPSO) by introducing oxygen and phosphorus into the Na_3SbS_4 sulfide solid electrolyte and comprehensively characterized its properties. We successfully developed a sodium-ion solid electrolyte with high conductivity and stability toward metallic sodium through the examination of its chemical structure, electrochemical properties and overall electrochemical performance in a Na | SE | Na symmetric cell. These mixed oxygen sulfide solid electrolytes, with their unique glass structure, present a promising avenue for the development of safe, low-cost, high-energy, and long-lasting all-solid-state sodium batteries.

2. Experimental section

2.1. Materials

Powder samples of $\text{Na}_3\text{SbP}_{0.4x}\text{S}_{4-x}\text{O}_x$ ($0 < x \leq 0.5$) and $\text{Na}_3\text{PSb}_{0.4x}\text{S}_{4-x}\text{O}_x$ ($0 < x \leq 0.5$) were prepared using traditional solid-state sintering methods. A 45 mL zirconia tank containing 12 zirconia balls (10 mm diameter) was loaded with a reagent mixture consisting of Sb_2S_3 (99%), P_2O_5 (99%), Sb_2O_5 (99%), Na_2S (95%), and S (99.99%). The combined materials (5 g) were continuously and thoroughly ground for 20 h at a speed of 500 rpm. Subsequently, all precursors were treated under vacuum conditions at 270 °C for 10 h. Samples with the best performance were selected and further processed under vacuum at temperatures of 380 °C, 420 °C, and 500 °C for 10 h to synthesize solid electrolytes with high conductivity and excellent electrochemical stability.

2.2. Symmetrical battery assembly

Approximately 100 mg of electrolyte powder was placed between two stainless steel plates and pressed to form electrolyte particles with a diameter of 10 mm, applying a pressure of 240 MPa. Sodium tablets with a diameter of 10 mm were placed on both sides of the electrolyte pellets, and the electrolytes containing the sodium tablets were pressed together under a pressure of 100 MPa. The entire assembly process was conducted inside a glove box filled with argon gas for protection.

2.3. Structure and morphology characterization

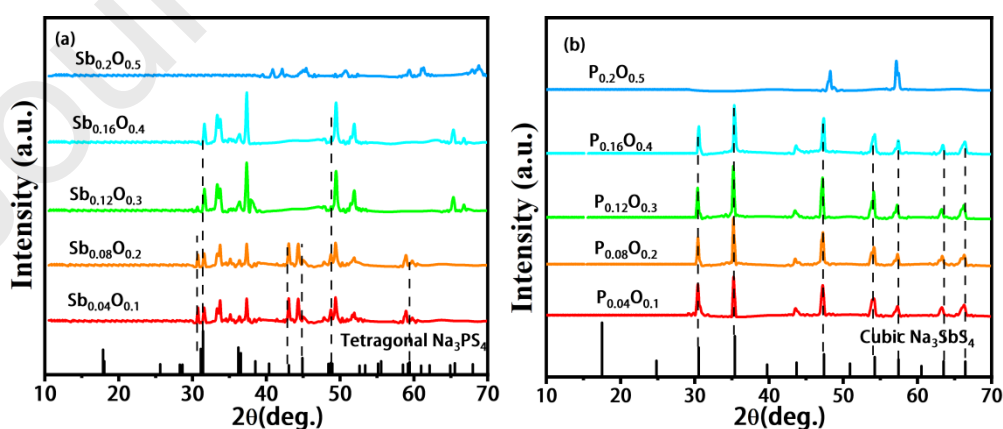
The phase structure of the solid electrolytes was investigated using X-ray diffraction (XRD, Bruker D2, Germany). XRD data were collected in the 2θ range of 10°–70° using Cu-K radiation, and the scanning was performed at 30 kV and 10 mA. The sample was placed in a polyimide-lined container during the XRD measurements to avoid contamination. Raman spectroscopy was used to investigate the chemical bond structure, utilizing an Ar^+ ion laser with an excitation wavelength of 785 nm. Raman scattering signals from the electrolyte sample were collected using a clear quartz plate within

a sealed container filled with dry Ar gas. Care was taken to transfer the materials from a dry Ar-filled container to the apparatus. Scanning electron microscopy (SEM) and energy-dispersive X-ray spectroscopy (EDS) analyses were conducted to examine the structure, elemental composition, and microstructure of the samples.

2.4 Electrochemical characterization

AC impedance measurements were performed using an electrochemical workstation (CHI660e) in the frequency range of 1 Hz to 10^6 Hz. Solid electrolyte materials were cold-pressed at 480 MPa into a depth of 0.6 mm and a diameter of 0.5 cm to fabricate the electrolyte plate. The cold-pressed electrolyte layers were sandwiched between two tempered steel sheets to serve as current collectors. Cell testing was conducted using a portable battery testing instrument (LAND CT2001). Prior to the tests, the cells were allowed to rest for 30 min to ensure the stability of the Na interface with the electrolytes. The charging and discharging phases were conducted with a current density of 0.05 mA cm^{-2} over a period of 0.5 h. H_2S emissions from the solid electrolyte were measured using a Pac 6500 H_2S gas sensor manufactured by Dräger Co. The powders (150 mg) were placed in a 2 L container maintained at 40% relative humidity (RH) and $26 \text{ }^\circ\text{C}$.

3. Results and discussion



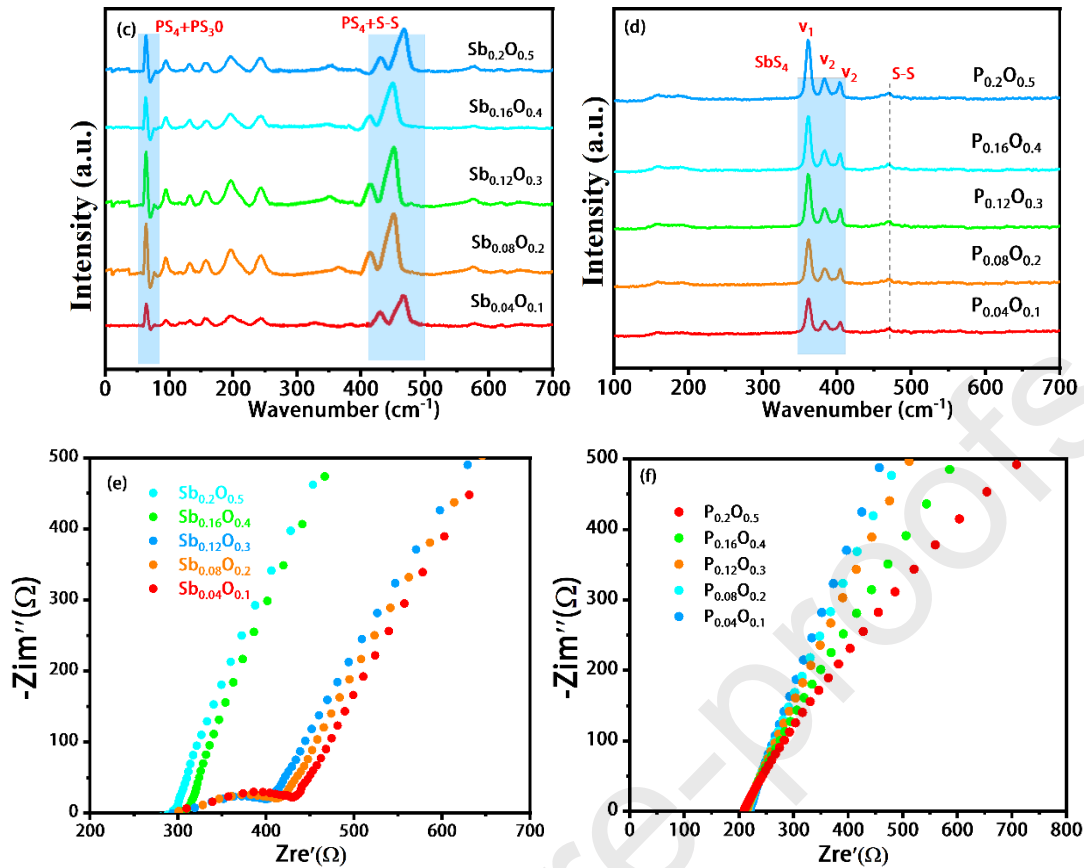


Fig. 1. XRD spectra of (a) $Na_3PSb_{0.4x}S_{4-x}O_x$ ($0 < x \leq 0.5$) and (b) $Na_3SbP_{0.4y}S_{4-y}O_y$ ($0 < y \leq 0.5$) after 20 h of mechanical milling and 10 h of heat treatment at 270 °C. Raman spectroscopy of (c) $Na_3PSb_{0.4x}S_{4-x}O_x$ ($0 < x \leq 0.5$) and (d) $Na_3SbP_{0.4y}S_{4-y}O_y$ ($0 < y \leq 0.5$) after 20 h of mechanical milling and 10 h of heat treatment at 270 °C. Nyquist impedance graphs of materials containing varying amounts of (e) $Sb_{0.4x}O_x$ and (f) $P_{0.4y}O_x$ ($0 < x \leq 0.5$) after 20 h of mechanical milling and 10 h of heat treatment at 270 °C.

To explore the optimal synthesis method for oxygen sulfur compound electrolytes containing Na, Sb, P, S, and O, we designed two electrolyte samples based on Na_3PS_4 and Na_3SbS_4 crystals. Figs. 1(a) and (b) show the different XRD patterns of $Na_3PSb_{0.4x}S_{4-x}O_x$ and $Na_3SbP_{0.4y}S_{4-y}O_y$ ($0 < y \leq 0.5$) after high-energy ball milling and heat treatment at 270 °C. The XRD spectrum of the $Na_3PSb_{0.4x}S_{4-x}O_x$ system indicated a tetragonal crystal structure of Na_3PS_4 with minor impurities[11]. These findings were consistent with previous research, suggesting possible amorphous nature during ball milling and heating, with impurity peaks corresponding to Na_3P and $Na_3PS_{4-x}O_x$ ($x = 1, 2, 3$). Although some degree of crystallinity was observed from these peaks, the

sample primarily consisted of tetragonal Na_3PS_4 . For $\text{Na}_3\text{SbP}_{0.4x}\text{S}_{4-x}\text{O}_x$ ($0 < x \leq 0.5$) samples with the same elemental composition, the XRD pattern compared with the PDF standard card revealed the main phase as the cubic phase of Na_3SbS_4 with a space group P-412c[12]. Each cell comprised nine SbS_4 segments, with Sb atoms positioned at 2a and S atoms located at 8e, providing a rapid Na^+ conduction pathway through the diffusion channel of the SbS_4 tetrahedron[13]. Although $\text{Na}_3\text{SbP}_{0.4x}\text{S}_{4-x}\text{O}_x$ exhibited a more favorable structure than $\text{Na}_3\text{PSb}_{0.4x}\text{S}_{4-x}\text{O}_x$, the 17° degree diffraction peak did not show the presence of cubic phase Na_3SbS_4 . This suggested that the heat treatment temperature may play a role, as previous studies indicated that cubic phase of Na_3SbS_4 requires temperatures[14]. Figs. 1(c) and (d) utilize Raman spectroscopy to investigate the chemical structure composition of the two sample groups. In Fig. 1(c), the main characteristic peak at 420 cm^{-1} corresponded to the stretching mode of the PS_4^{2-} unit, which represented a non bridged sulfur unit[10]. The P^1 unit reflected the number of bridging oxygen, and the superscripts indicated the number of short-range ordered units. The original P^0 unit undergoes a disproportionation process upon the addition of oxygen, leading to the generation of sodium sulfide ($2\text{P}^0 \rightarrow 2\text{P}^1 + \text{Na}_2\text{S}$) to maintain charge balance. The introduction of oxygen is clearly observed through the peaks attributed to the formation of mixed oxygen sulfide and oxide units, such as PS_2O_2 oxygen sulfide (83 ppm) and PSO_3 oxygen sulfide (50 ppm)[15]. The appearance of $\text{PS}_{4-x}\text{O}_x$ oxygen sulfide units indicates the injection of oxygen into the P–S tetrahedral units. Compared with the P–S bond, the P–O has stronger chemical bond energy. Additionally, the presence of bridging oxygen can contribute to a more stable and uniform glass network in the unit microstructure[16]. As shown in Fig. 2(d), a standard SbS_4 structural unit was formed at 380 cm^{-1} for the sample $\text{Na}_3\text{SbP}_{0.4x}\text{S}_{4-x}\text{O}_x$. Furthermore, the –S–S– link from P_2S_6 defect unit produced during the disproportionation process exhibited characteristic Raman modes at 460 cm^{-1} . This observation was consistent with the reaction ($2\text{P}^0 \rightarrow 2\text{P}^1 + \text{Na}_2\text{S}$) presented in $\text{Na}_3\text{PSb}_{0.4x}\text{S}_{4-x}\text{O}_x$. AC impedance tests were conducted on the samples to further demonstrate the superiority of the P–O structure. $\text{Na}_3\text{PSb}_{0.4x}\text{S}_{4-x}\text{O}_x$ displays a half circle and a 45° angled straight line in the Nyquist plot of Fig. 1(e). The semicircle in the high-frequency zone represented the charge transfer

resistance arising from diffusion between the electrode and electrolyte[17]. The low-frequency straight line, known as Warburg impedance or concentration polarization impedance, relates to the movement of sodium ions between the electrodes. With an increase in the O and Sb content, the transfer impedance of the electrolyte decreased. These observations suggested that sodium ion conduction essentially controlled the battery's dynamic response process[18]. This can be explained by an increase in the Sb element, resulting in the formation of the sodium ion-conducting Na_3SbS_4 structure. Impedance R_t is related to room-temperature conductivity (σ_{25}) and can be determined using the following equation: $\sigma(\text{ms cm}^{-1}) = L/SR_t$, where L denotes the sample thickness, and S denotes the circular area between the electrode and the electrolyte. The conductivity of $\text{Na}_3\text{SbP}_{0.2}\text{S}_{3.5}\text{O}_{0.5}$ was determined to be 0.254 mS cm^{-1} . By contrast, Fig. 1(f) depicts the $\text{Na}_3\text{SbP}_{0.4x}\text{S}_{4-x}\text{O}_x$ samples with the same elemental composition but improved conductivity due to the formation of the main phase of Na_3SbS_4 , reaching a maximum of 0.382 mS cm^{-1} with negligible transfer impedance. Tables 1 and 2 show the material performance data of all samples at $270 \text{ }^\circ\text{C}$. As expected, P and O elements undergo disproportionation reaction, releasing Na_2S_x , which is consistent with previous research indicating the enhanced role of the P–O structure in electrochemical stability. The $\text{Na}_3\text{SbP}_{0.4x}\text{S}_{4-x}\text{O}_x$ electrolyte with a cubic phase Na_3SbS_4 structure demonstrated remarkably improved conductivity while maintaining excellent stability[19].

Table 1

Electrochemical performance of $\text{Na}_3\text{PSb}_{0.4x}\text{S}_{4-x}\text{O}_x$ electrolyte treated at $270 \text{ }^\circ\text{C}$

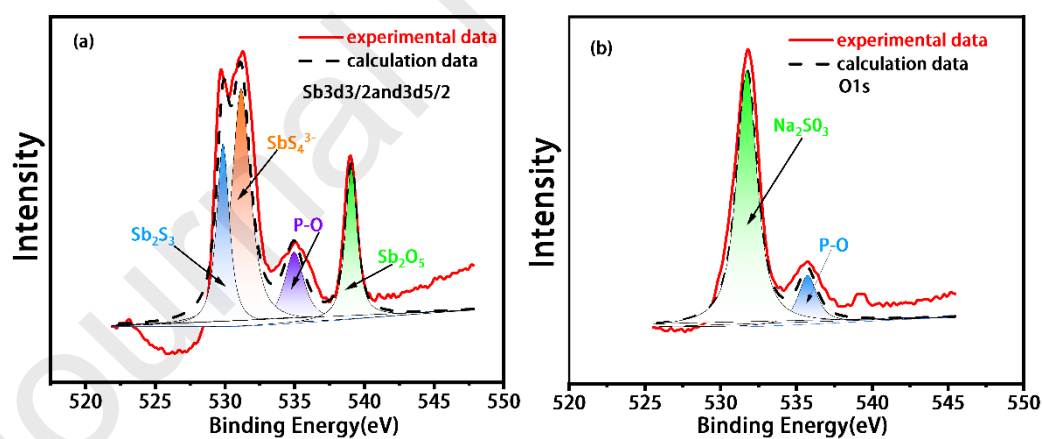
composition	Impedance	electron conductivity	Ionic conductivity	H_2S release
Na_3PS_4	443 Ω	$3.33 \times 10^{-5} \text{ mS cm}^{-1}$	0.201 mS cm^{-1}	$1.88 \text{ cm}^3 \text{ g}^{-1}$
$\text{Na}_3\text{PSb}_{0.04}\text{S}_4\text{O}_{0.1}$	431.1 Ω	$3.82 \times 10^{-5} \text{ mS cm}^{-1}$	0.206 mS cm^{-1}	$1.899 \text{ cm}^3 \text{ g}^{-1}$
$\text{Na}_3\text{PSb}_{0.08}\text{S}_4\text{O}_{0.2}$	413.4 Ω	$3.12 \times 10^{-5} \text{ mS cm}^{-1}$	0.215 mS cm^{-1}	$1.68 \text{ cm}^3 \text{ g}^{-1}$
$\text{Na}_3\text{PSb}_{0.12}\text{S}_4\text{O}_{0.3}$	401.3 Ω	$2.3 \times 10^{-5} \text{ mS cm}^{-1}$	0.222 mS cm^{-1}	$1.53 \text{ cm}^3 \text{ g}^{-1}$

$\text{Na}_3\text{PSb}_{0.16}\text{S}_4\text{O}_{0.4}$	315 Ω	5.02×10^{-6} mS cm^{-1}	0.283 mS cm^{-1}	$1.38 \text{ cm}^3 \text{ g}^{-1}$
$\text{Na}_3\text{PSb}_{0.2}\text{S}_4\text{O}_{0.5}$	300.8 Ω	8.56×10^{-5} mS cm^{-1}	0.254 mS cm^{-1}	$1.12 \text{ cm}^3 \text{ g}^{-1}$

Table 2

Electrochemical performance of $\text{Na}_3\text{SbP}_{0.4x}\text{S}_{4-x}\text{O}_x$ electrolyte treated at 270 °C

composition	Impedance	electron conductivity	Ionic conductivity	H_2S release
Na_3SbS_4	223.6 Ω	4.32×10^{-5} mS cm^{-1}	0.398 mS cm^{-1}	$1.37 \text{ cm}^3 \text{ g}^{-1}$
$\text{Na}_3\text{SbP}_{0.04}\text{S}_4\text{O}_{0.1}$	220.37 Ω	5.6×10^{-5} mS cm^{-1}	0.304 mS cm^{-1}	$0.888 \text{ cm}^3 \text{ g}^{-1}$
$\text{Na}_3\text{SbP}_{0.08}\text{S}_4\text{O}_{0.2}$	216.48 Ω	3.4×10^{-5} mS cm^{-1}	0.311 mS cm^{-1}	$0.9 \text{ cm}^3 \text{ g}^{-1}$
$\text{Na}_3\text{SbP}_{0.12}\text{S}_4\text{O}_{0.3}$	214.61 Ω	5.1×10^{-5} mS cm^{-1}	0.382 mS cm^{-1}	$0.912 \text{ cm}^3 \text{ g}^{-1}$
$\text{Na}_3\text{SbP}_{0.16}\text{S}_4\text{O}_{0.4}$	212.73 Ω	4.13×10^{-5} mS cm^{-1}	0.319 mS cm^{-1}	$0.78 \text{ cm}^3 \text{ g}^{-1}$
$\text{Na}_3\text{SbP}_{0.2}\text{S}_4\text{O}_{0.5}$	211.08 Ω	3.6×10^{-5} mS cm^{-1}	0.322 mS cm^{-1}	$0.53 \text{ cm}^3 \text{ g}^{-1}$



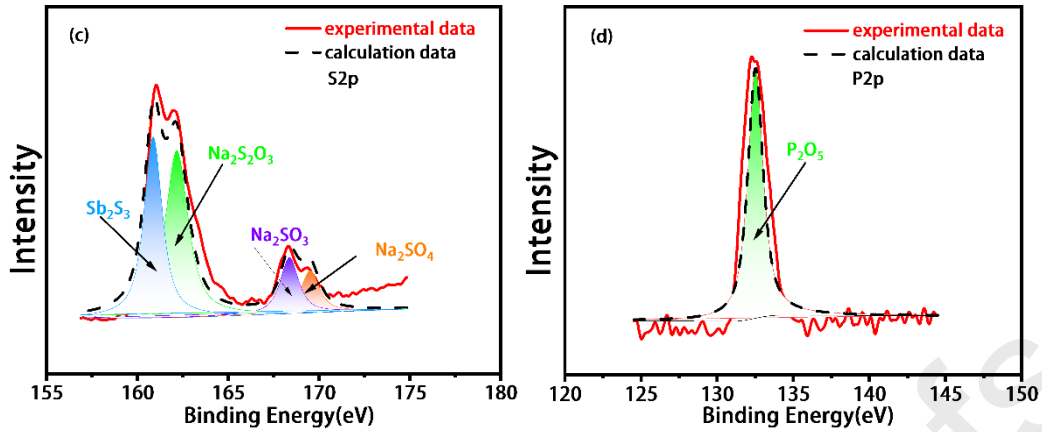


Fig. 2. X-ray photoelectron spectroscopy (XPS) spectra of (a) $\text{Na}_3\text{SbP}_{0.16}\text{S}_{3.6}\text{O}_{0.4}$ solid electrolyte with deconvoluted Sb3d spectra. (b) $\text{Na}_3\text{SbP}_{0.16}\text{S}_{3.6}\text{O}_{0.4}$ solid electrolyte with deconvoluted O1s spectra. (c) $\text{Na}_3\text{SbP}_{0.16}\text{S}_{3.6}\text{O}_{0.4}$ solid electrolyte with deconvoluted S2p spectra. (d) $\text{Na}_3\text{SbP}_{0.16}\text{S}_{3.6}\text{O}_{0.4}$ solid electrolyte with deconvoluted P2p spectra.

XPS analysis was performed to examine the surface of the $\text{Na}_3\text{SbP}_{0.16}\text{S}_{3.6}\text{O}_{0.4}$ -270 °C electrolyte (Fig. 2). The Sb 3d_{5/2} and 3d_{3/2} peaks were detected at 539 and 531 eV, respectively. The split peak of Sb 3d_{3/2} (531 eV) indicated the formation of distinct binding energy modes[1], specifically the P–O structure in the electrolyte. The presence of Sb element ion groups with different valence states in electrolyte samples can be considered as a disadvantage for the formation of the electrolyte due to low temperature treatment. A broad peak of Sb 3d_{3/2} was observed for this structure due to the overlap with the O 1s (531.8 eV) peak. The P–O structure can be clearly observed in the deconvolution spectrum. The S and P 2p spectra of the pellets were observed at 160.9 and 132.4 eV, respectively[20]. In accordance with the research by Tian et al[21]. and Wenzel et al[22]., Due to the doping of oxygen elements, although at low temperatures, these 2p peak pairs of S and P corresponded to the reduced phosphide and sulfide species, respectively. However, they were incompatible with Na metal batteries due to their nature as combined ion and electron conductors, as they tended to form unstable solid electrolyte interphases (SEIs), despite their high ionic conductivity.

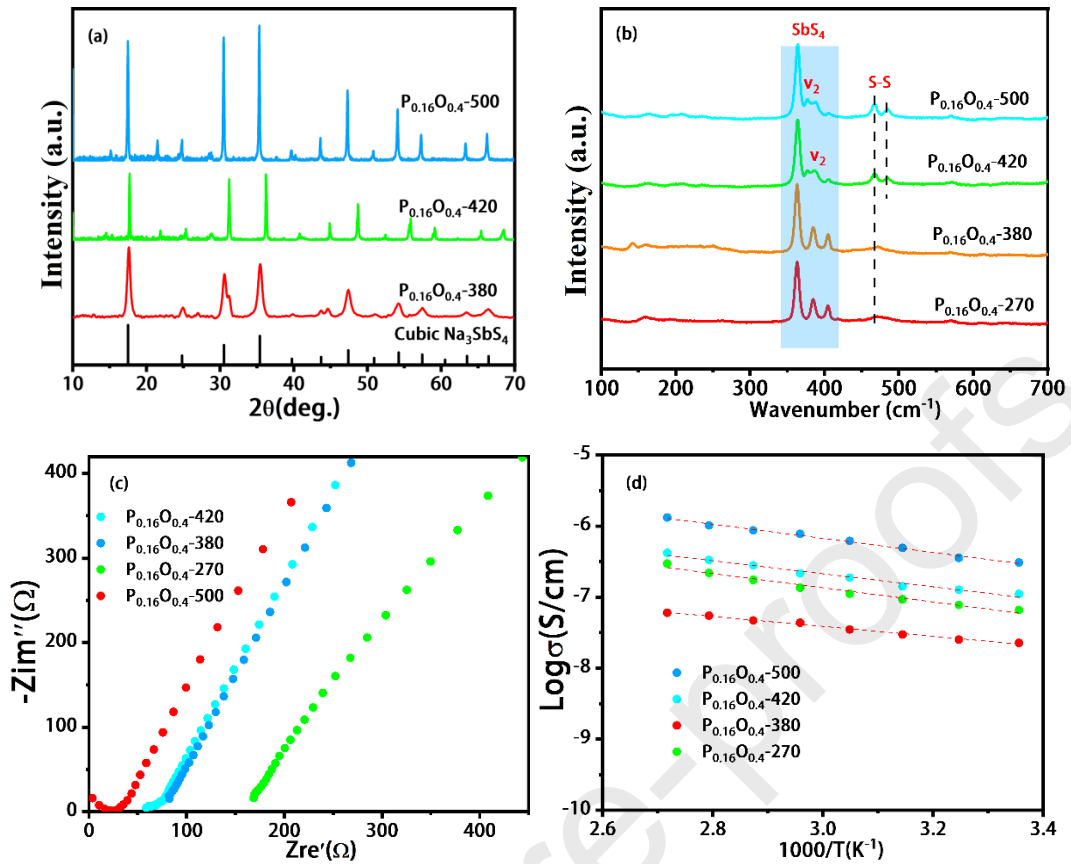


Fig. 3. (a) XRD spectra and (b) Raman spectrum of the $\text{Na}_3\text{SbP}_{0.16}\text{S}_{3.6}\text{O}_{0.4}$ electrolyte under different temperature treatments. (c) Nyquist plots of the electrolyte under different temperature treatments. (d) Arrhenius of the electrolyte₄ after treatment at different temperatures.

The ion conductivity of $\text{Na}_3\text{SbP}_{0.4x}\text{S}_{4-x}\text{O}_x$ was further improved to develop solid-state batteries with excellent performance. Increasing the temperature of the Na_3SbS_4 electrolyte was the most effective approach to enhance ion conductivity. The XRD spectrum in Fig. 3(a) demonstrates the structural information of the $\text{Na}_3\text{SbP}_{0.16}\text{S}_{3.6}\text{O}_{0.4}$ sample after heating treatment. when the electrolyte treatment temperature reached 380 °C[23], a complete cubic phase Na_3SbS_4 XRD diffraction pattern was observed, with a prominent peak centered at 17°. As the temperature continued to rise, the intensity of the diffraction peaks remarkably increased[24]. At 500 °C, the prominent diffraction peaks were obviously strengthened, confirming their highly crystalline structure. However, a few impurity peaks were observed at high temperatures, identified as NaS_x produced by the disproportionation reaction of the P–O structure. The Raman spectrum in Fig. 3(b) demonstrates that the electrolytes $\text{Na}_3\text{SbP}_{0.16}\text{S}_{3.4}\text{O}_{0.4-270}$ and $\text{Na}_3\text{SbP}_{0.16}\text{S}_{3.4}\text{O}_{0.4-380}$ exhibited strong SbS_4 tensile vibration modes at 360, 380, and

410 cm^{-1} . With increasing temperature, the V_2 vibration peak weakened, and the formation of $-\text{S}-\text{S}-$ was observed[25], consistent with the results from the XRD analysis. The temperature rise accelerated the disproportionation reaction ($2\text{P}^0 \rightarrow 2\text{P}^1 + \text{Na}_2\text{S}$) and facilitated the growth of Na_3SbS_4 cubic phase crystals. Additionally, the incorporation of oxygen led to the formation of more bridging oxygen structures and the potential emergence of a Na_2S phase with low conductivity[26]. The overall electrochemical performance was remarkably increased, with the impedance of $\text{Na}_3\text{SbP}_{0.16}\text{S}_{3.6}\text{O}_{0.4}$ -500 reduced to 20.9 Ω at ambient temperature. Fig. 3(c) shows the Nyquist profile of $\text{Na}_3\text{SbP}_{0.16}\text{S}_{3.6}\text{O}_{0.4}$ -500 electrolyte, exhibiting a semicircle in the high-frequency region, which further supports the occurrence of P–O structural disproportionation reaction[27]. The calculated ion conductivity for this sample. Fig. 3(d) illustrates the effect of temperature on ion conductivity of the aforementioned electrolyte, with a room temperature conductivity of 3.82 mS cm^{-1} . Tables 3 - 8 show the material performance data of all samples at 380 $^\circ\text{C}$, 420 $^\circ\text{C}$ and 500 $^\circ\text{C}$. The materials were evaluated over a temperature range of 30 $^\circ\text{C}$ to 100 $^\circ\text{C}$, revealing a linear relationship between $\log 1000/T$ and temperature. The activation energy E_a was determined using the formula $\sigma = \sigma_0 e^{-(E_a/k_B T)}$, where σ_0 represents the pre-exponential parameter, and k_B is the Boltzmann constant. The $\text{Na}_3\text{SbP}_{0.16}\text{S}_{3.6}\text{O}_{0.4}$ -500 electrolyte exhibited a minimum E_a of 0.991 eV. The increased activation energy can be attributed to the formation of more BO units, resulting in structural contraction in response to oxygen incorporation, which subsequently reduces the available free volume for conduction. In addition, the enhanced growth of Na_3SbS_4 crystals under high-temperature heat treatment contributes to the high ion conductivity[28].

Table 3

Electrochemical performance of $\text{Na}_3\text{PSb}_{0.4x}\text{S}_{4-x}\text{O}_x$ electrolyte treated at 380 $^\circ\text{C}$

composition	Impedance	electron conductivity	Ionic conductivity	H_2S release
Na_3PS_4	343 Ω	$6.21 \times 10^{-5} \text{ mS cm}^{-1}$	0.26 mS cm^{-1}	1.02 $\text{cm}^3 \text{ g}^{-1}$

$\text{Na}_3\text{PSb}_{0.04}\text{S}_4\text{O}_{0.1}$	331.1 Ω	5.2×10^{-5} mS cm^{-1}	0.269 mS cm^{-1}	1.29 $\text{cm}^3 \text{g}^{-1}$
$\text{Na}_3\text{PSb}_{0.08}\text{S}_4\text{O}_{0.2}$	239.4 Ω	5.12×10^{-5} mS cm^{-1}	0.372 mS cm^{-1}	1.6 $\text{cm}^3 \text{g}^{-1}$
$\text{Na}_3\text{PSb}_{0.12}\text{S}_4\text{O}_{0.3}$	222.3 Ω	3.23×10^{-5} mS cm^{-1}	0.401 mS cm^{-1}	1.31 $\text{cm}^3 \text{g}^{-1}$
$\text{Na}_3\text{PSb}_{0.16}\text{S}_4\text{O}_{0.4}$	251 Ω	6.02×10^{-5} mS cm^{-1}	0.355 mS cm^{-1}	1.3 $\text{cm}^3 \text{g}^{-1}$
$\text{Na}_3\text{PSb}_{0.2}\text{S}_4\text{O}_{0.5}$	260.3 Ω	4.56×10^{-5} mS cm^{-1}	0.342 mS cm^{-1}	1.1 $\text{cm}^3 \text{g}^{-1}$

Table 4

Electrochemical performance of $\text{Na}_3\text{SbP}_{0.4x}\text{S}_{4-x}\text{O}_x$ electrolyte treated at 380 °C

composition	Impedance	electron conductivity	Ionic conductivity	H_2S release
Na_3SbS_4	223.6 Ω	4.29×10^{-5} mS cm^{-1}	0.398 mS cm^{-1}	0.98 $\text{cm}^3 \text{g}^{-1}$
$\text{Na}_3\text{SbP}_{0.04}\text{S}_4\text{O}_{0.1}$	220.37 Ω	4.6×10^{-5} mS cm^{-1}	0.404 mS cm^{-1}	0.73 $\text{cm}^3 \text{g}^{-1}$
$\text{Na}_3\text{SbP}_{0.08}\text{S}_4\text{O}_{0.2}$	216.48 Ω	3.98×10^{-5} mS cm^{-1}	0.411 mS cm^{-1}	0.8 $\text{cm}^3 \text{g}^{-1}$
$\text{Na}_3\text{SbP}_{0.12}\text{S}_4\text{O}_{0.3}$	214.61 Ω	4.17×10^{-5} mS cm^{-1}	0.415 mS cm^{-1}	0.81 $\text{cm}^3 \text{g}^{-1}$
$\text{Na}_3\text{SbP}_{0.16}\text{S}_4\text{O}_{0.4}$	82.4 Ω	3.05×10^{-5} mS cm^{-1}	1.08 mS cm^{-1}	0.53 $\text{cm}^3 \text{g}^{-1}$
$\text{Na}_3\text{SbP}_{0.2}\text{S}_4\text{O}_{0.5}$	211.08 Ω	3.6×10^{-5} mS cm^{-1}	0.422 mS cm^{-1}	0.69 $\text{cm}^3 \text{g}^{-1}$

Table 5

Electrochemical performance of $\text{Na}_3\text{PSb}_{0.4x}\text{S}_{4-x}\text{O}_x$ electrolyte treated at 420 °C

composition	Impedance	electron conductivity	Ionic conductivity	H_2S release
Na_3PS_4	243 Ω	2.8×10^{-5} mS cm^{-1}	0.367 mS cm^{-1}	1.18 $\text{cm}^3 \text{g}^{-1}$
$\text{Na}_3\text{PSb}_{0.04}\text{S}_4\text{O}_{0.1}$	231.1 Ω	3.2×10^{-5} mS cm^{-1}	0.385 mS cm^{-1}	1.09 $\text{cm}^3 \text{g}^{-1}$
$\text{Na}_3\text{PSb}_{0.08}\text{S}_4\text{O}_{0.2}$	213.4 Ω	2.12×10^{-5} mS cm^{-1}	0.417 mS cm^{-1}	1.37 $\text{cm}^3 \text{g}^{-1}$
$\text{Na}_3\text{PSb}_{0.12}\text{S}_4\text{O}_{0.3}$	201.3 Ω	3.02×10^{-5} mS cm^{-1}	0.442 mS cm^{-1}	1.26 $\text{cm}^3 \text{g}^{-1}$
$\text{Na}_3\text{PSb}_{0.16}\text{S}_4\text{O}_{0.4}$	215 Ω	2.15×10^{-5} mS cm^{-1}	0.414 mS cm^{-1}	1.56 $\text{cm}^3 \text{g}^{-1}$

Na₃PSb_{0.2}S₄O_{0.5} 200.8 Ω 4.6×10⁻⁵ mS cm⁻¹ 0.444 mS cm⁻¹ 1.35 cm³ g⁻¹

Table 6

Electrochemical performance of Na₃SbP_{0.4x}S_{4-x}O_x electrolyte treated at 420 °C

composition	Impedance	electron conductivity	Ionic conductivity	H ₂ S release
Na ₃ SbS ₄	123.6 Ω	4.32×10 ⁻⁵ mS cm ⁻¹	0.721 mS cm ⁻¹	0.9 cm ³ g ⁻¹
Na ₃ SbP _{0.04} S ₄ O _{0.1}	120.37 Ω	5.6×10 ⁻⁵ mS cm ⁻¹	0.74 mS cm ⁻¹	0.73 cm ³ g ⁻¹
Na ₃ SbP _{0.08} S ₄ O _{0.2}	116.48 Ω	3.4×10 ⁻⁵ mS cm ⁻¹	0.765 mS cm ⁻¹	0.7 cm ³ g ⁻¹
Na ₃ SbP _{0.12} S ₄ O _{0.3}	114.61 Ω	5.1×10 ⁻⁵ mS cm ⁻¹	0.778 mS cm ⁻¹	0.62 cm ³ g ⁻¹
Na ₃ SbP _{0.16} S ₄ O _{0.4}	66.2 Ω	4.13×10 ⁻⁵ mS cm ⁻¹	1.34 mS cm ⁻¹	0.442 cm ³ g ⁻¹
Na ₃ SbP _{0.2} S ₄ O _{0.5}	73.08 Ω	3.6×10 ⁻⁵ mS cm ⁻¹	1.22 mS cm ⁻¹	0.65 cm ³ g ⁻¹

Table 7

Electrochemical performance of Na₃PSb_{0.4x}S_{4-x}O_x electrolyte treated at 500 °C

composition	Impedance	electron conductivity	Ionic conductivity	H ₂ S release
Na ₃ PS ₄	84 Ω	3.53×10 ⁻⁵ mS cm ⁻¹	1.06 mS cm ⁻¹	2.3 cm ³ g ⁻¹
Na ₃ PSb _{0.04} S ₄ O _{0.1}	51.1 Ω	2.25×10 ⁻⁵ mS cm ⁻¹	1.74 mS cm ⁻¹	2.01 cm ³ g ⁻¹
Na ₃ PSb _{0.08} S ₄ O _{0.2}	43.4 Ω	3.51×10 ⁻⁵ mS cm ⁻¹	2.05 mS cm ⁻¹	1.88 cm ³ g ⁻¹
Na ₃ PSb _{0.12} S ₄ O _{0.3}	40.3Ω	3.34×10 ⁻⁵ mS cm ⁻¹	2.21 mS cm ⁻¹	1.93 cm ³ g ⁻¹
Na ₃ PSb _{0.16} S ₄ O _{0.4}	55Ω	5.6×10 ⁻⁵ mS cm ⁻¹	1.62 mS cm ⁻¹	1.54 cm ³ g ⁻¹
Na ₃ PSb _{0.2} S ₄ O _{0.5}	50.8 Ω	3.53×10 ⁻⁵ mS cm ⁻¹	1.75 mS cm ⁻¹	2.1 cm ³ g ⁻¹

Table 8

Electrochemical performance of Na₃SbP_{0.4x}S_{4-x}O_x electrolyte treated at 500 °C

composition	Impedance	electron conductivity	Ionic conductivity	H ₂ S release
-------------	-----------	-----------------------	--------------------	--------------------------

Na_3SbS_4	43.6 Ω	5.0×10^{-5} mS cm^{-1}	2.03 mS cm^{-1}	1.02 $\text{cm}^3 \text{g}^{-1}$
$\text{Na}_3\text{SbP}_{0.04}\text{S}_4\text{O}_{0.1}$	22.37 Ω	4.98×10^{-5} mS cm^{-1}	3.41 mS cm^{-1}	0.6 $\text{cm}^3 \text{g}^{-1}$
$\text{Na}_3\text{SbP}_{0.08}\text{S}_4\text{O}_{0.2}$	33.48 Ω	4.36×10^{-5} mS cm^{-1}	2.66 mS cm^{-1}	0.56 $\text{cm}^3 \text{g}^{-1}$
$\text{Na}_3\text{SbP}_{0.12}\text{S}_4\text{O}_{0.3}$	21.61 Ω	4.1×10^{-5} mS cm^{-1}	3.53 mS cm^{-1}	0.412 $\text{cm}^3 \text{g}^{-1}$
$\text{Na}_3\text{SbP}_{0.16}\text{S}_4\text{O}_{0.4}$	21.09 Ω	4.35×10^{-5} mS cm^{-1}	3.82 mS cm^{-1}	0.202 $\text{cm}^3 \text{g}^{-1}$
$\text{Na}_3\text{SbP}_{0.2}\text{S}_4\text{O}_{0.5}$	32.08 Ω	7.64×10^{-5} mS cm^{-1}	2.38 mS cm^{-1}	0.342 $\text{cm}^3 \text{g}^{-1}$

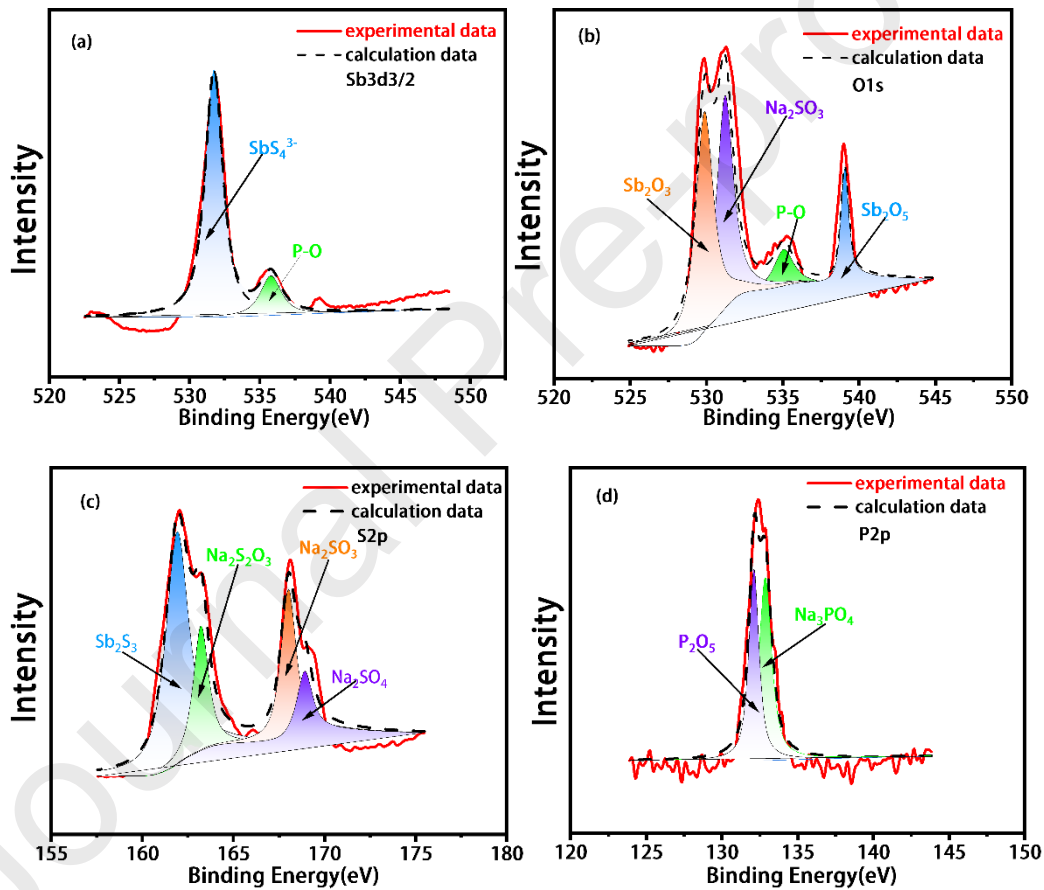


Fig. 4. XPS spectra of (a) $\text{Na}_3\text{SbP}_{0.16}\text{S}_{3.6}\text{O}_{0.4}$ -500 solid electrolyte with deconvoluted Sb3d spectra. (b) $\text{Na}_3\text{SbP}_{0.16}\text{S}_{3.6}\text{O}_{0.4}$ solid electrolyte with deconvoluted O1s spectra. (c) $\text{Na}_3\text{SbP}_{0.16}\text{S}_{3.6}\text{O}_{0.4}$ solid electrolyte with deconvoluted S2p spectra. (d) $\text{Na}_3\text{SbP}_{0.16}\text{S}_{3.6}\text{O}_{0.4}$ solid electrolyte with deconvoluted P2p spectra.

XPS was utilized to determine the elemental composition of the $\text{Na}_3\text{SbP}_{0.16}\text{S}_{3.6}\text{O}_{0.4}$ -500 solid electrolyte. In Fig. 4(a), only the Sb 3d3/2 peak with a binding energy at 531.7 eV is observed. As the temperature increases, the formation of more Na_3SbS_4 crystals

is evident, indicating the absence of insufficiently reacted Sb element ion groups and accounting for the different energy peak compared with the sample before heat treatment. Moreover, an additional O1s binding energy at 540 eV is observed in Fig. 4(b), alongside the O1s binding energy peak at 531.7 eV. This suggests a linear increase in the proportion of BO species with increasing O content in the NaSbPSO electrolyte. High temperature treatment promotes this disproportionation reaction ($2P^0 \rightarrow 2P^1 + Na_2S$), resulting in the production of more oxygen and sulfur compounds in the electrolyte. Spectral deconvolution of $Na_3SbP_{0.16}S_{3.6}O_{0.4-500}$ revealed that the majority of the extra oxygen atoms were incorporated into the electrolyte as bridging oxygen, as evidenced by the O1s binding energy outside of 531.7 eV[29]. The shoulder in the S 2p spectrum shifts to a higher binding energy in Fig. 4(c). This shift can be attributed to the polarization of sulfur atoms originally bonded with phosphorus due to the increased oxygen bonding, resulting in the transfer of sulfur to higher binding energies. This corresponds to the formation of $-S-S-$ sulfur species in the shape of Na_2S on the NSbPSO electrolyte. In addition, the absence of the shoulder in this spectrum indicates that prior to the reaction, more covalent S-sulfur molecules were replaced by more $-S-S-$ sulfur species[30]. The P 2p XPS spectra of $Na_3SbP_{0.16}S_{3.6}O_{0.4-500}$ and $Na_3SbP_{0.16}S_{3.6}O_{0.4-270}$ exhibit no significant difference, indicating the lack of Na_3P generation or the presence of fewer Na_3P_x in these samples[21]. However, the binding energy of P-O compounds appeared in $Na_3SbP_{0.16}S_{3.6}O_{0.4-500}$, further supporting the fact of the disproportionation reaction between P and O elements in the electrolyte.

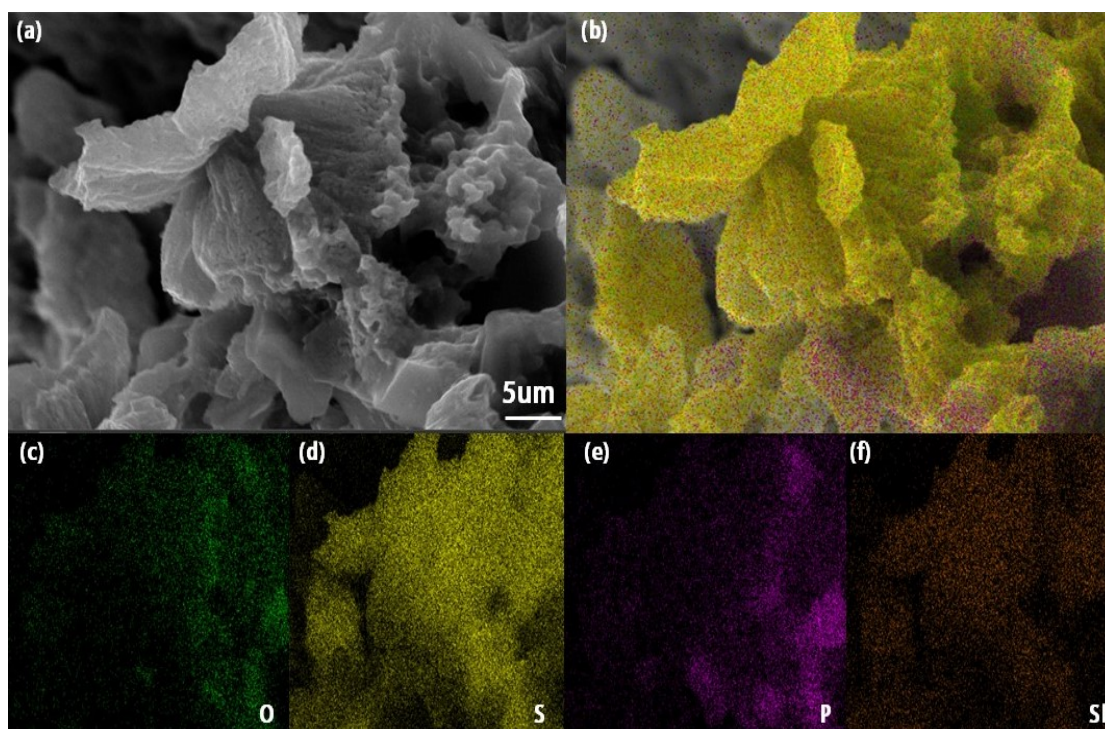


Fig. 5. (a) SEM images of the $\text{Na}_3\text{SbP}_{0.16}\text{S}_{3.6}\text{O}_{0.4-500}$ sample at 5 μm magnification. (b) EDAX mapping area of $\text{Na}_3\text{SbP}_{0.16}\text{S}_{3.6}\text{O}_{0.4-500}$ and (c–f) individual elemental mapping of O, S, P, and Sb.

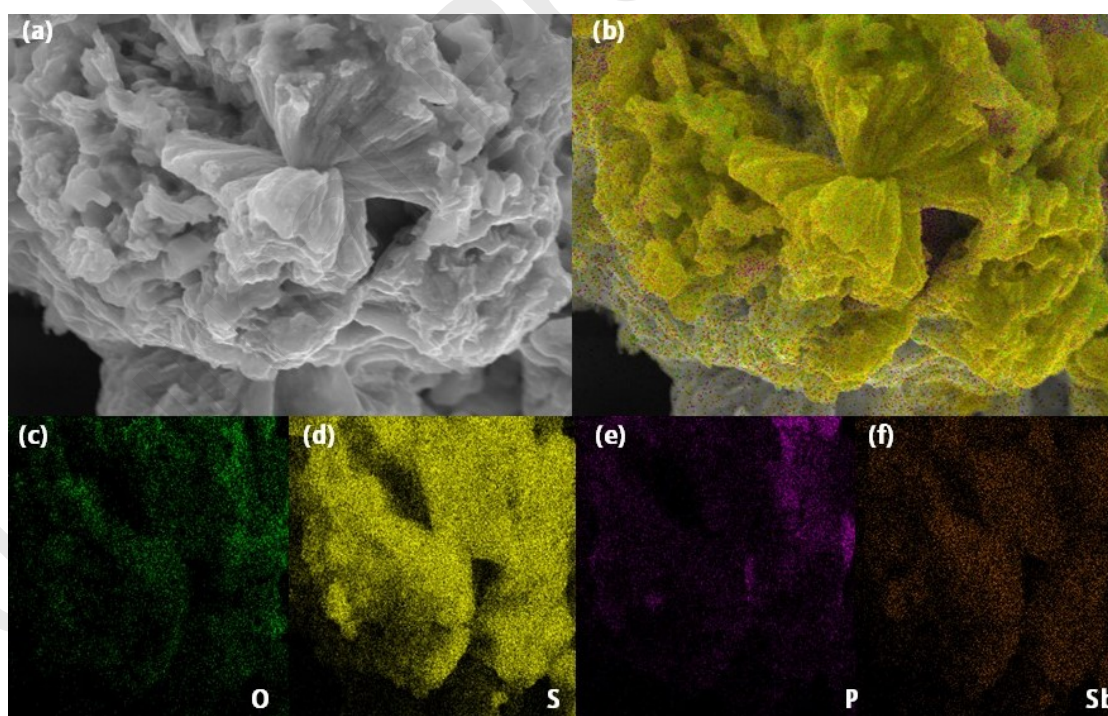


Fig. 6. (a) SEM images of the $\text{Na}_3\text{SbP}_{0.16}\text{S}_{3.6}\text{O}_{0.4-420}$ sample at 5 μm magnification. (b) EDAX mapping area of $\text{Na}_3\text{SbP}_{0.16}\text{S}_{3.6}\text{O}_{0.4-420}$ and (c–f) individual elemental mapping of O, S, P, and Sb.

Here, the microstructure of $\text{Na}_3\text{SbP}_{0.16}\text{S}_{3.6}\text{O}_{0.4-500}$ and $\text{Na}_3\text{SbP}_{0.16}\text{S}_{3.6}\text{O}_{0.4-420}$ was observed using field emission SEM images with EDS mapping. In the powder form,

the electrolyte exhibited a uniform porous flocculent structure. Within the electrolyte substance, these particles were dispersed randomly, resembling the often-found layered double hydroxide structure. These unique structural forms were a result of high-energy ball milling and high-temperature processing, and the structure was heavily affected by oxygen doping, resulting in tiny particles and agglomerated powders[31]. This structural characteristic is crucial for suppressing the propagation of Na dendrites. The EDS analysis of elements in the $\text{Na}_3\text{SbP}_{0.16}\text{S}_{3.6}\text{O}_{0.4-500}$ micro area is further shown in Figs. 5(b–f). The distribution of various elements is clearly depicted, with S and Sb elements accounting for the majority, indicating that the electrolyte is still a solid compound of Na_3SbS_4 .

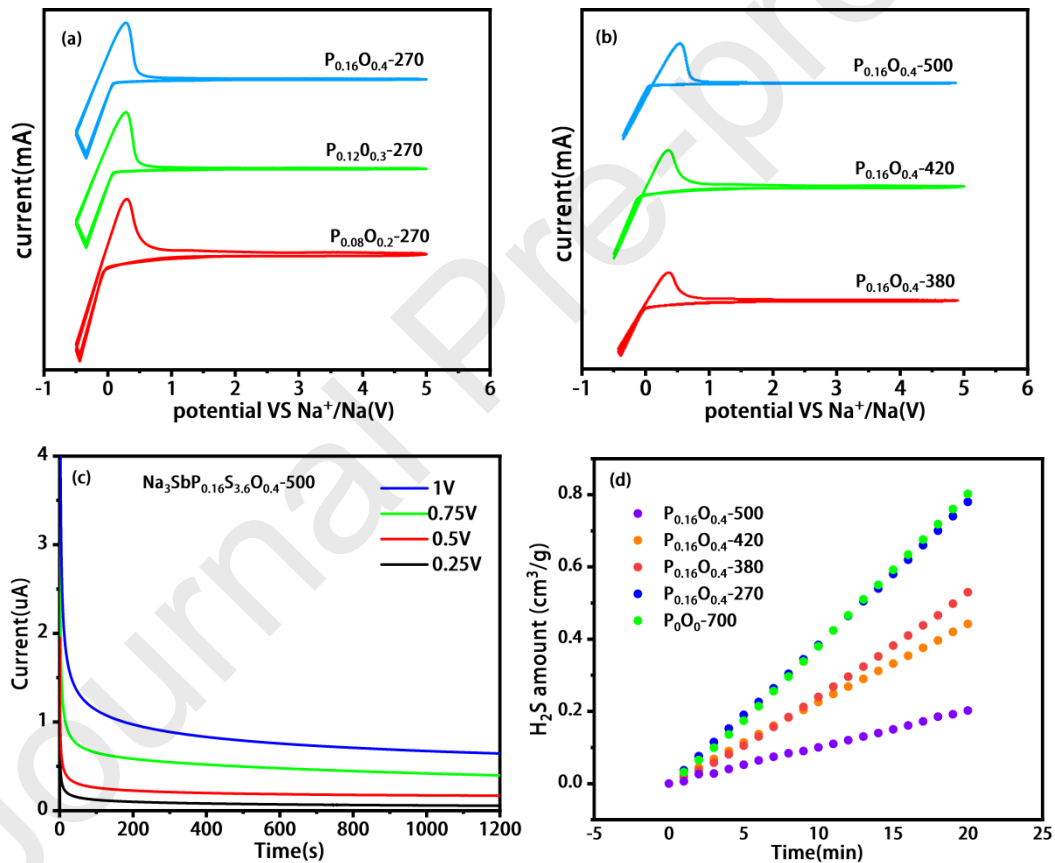


Fig. 7. (a) Cyclic voltammetry (CV) curves with a scanning rate of 1 mV/s for $\text{Na}_3\text{SbP}_{0.4x}\text{S}_{4-x}\text{O}_x$ ($0 < x \leq 0.5$) with different doping levels at 270 °C. (b) CV curves of $\text{Na}_3\text{SbP}_{0.16}\text{S}_{3.6}\text{O}_{0.4}$ at different heat treatment temperatures at a scanning rate of 1 mV/s. (c) Direct current polarization curves of $\text{Na}_3\text{SbP}_{0.16}\text{S}_{3.6}\text{O}_{0.4}$ with applied voltage at 25 °C. (d) Amount of H_2S produced after exposing $\text{Na}_3\text{SbP}_{0.16}\text{S}_{3.6}\text{O}_{0.4}$ to different heat treatment temperatures and humid air (RH = 40%) for 20 min.

The P–O structure-modified $\text{Na}_3\text{SbP}_{0.4x}\text{S}_{4-x}\text{O}_x$ solid electrolyte underwent testing for long-term electrochemical stability using CV (Figs. 6[a–b]). A standard sodium electrode and a stainless steel working electrode were used, and the electrolyte powder was compressed into blocks at a pressure of approximately 240 MPa. A semi enclosed battery was assembled using Na/SE/blocking electrodes[32]. The sodium adsorption and desorption processes were examined in low-potential (below 1 V) electrochemical oxidation and reduction reactions. Under the low-temperature treatment of $\text{Na}_3\text{SbP}_{0.16}\text{S}_{3.6}\text{O}_{0.4}$, the reduction reaction under negative voltage was irreversible (Fig. 6[a]). By contrast, remarkable reversibility was observed in the high-temperature CV curves for the $\text{Na}_3\text{SbP}_{0.16}\text{S}_{3.6}\text{O}_{0.4}$ electrolyte (Fig. 6[b]). Additionally, the resulting solid electrolyte exhibited a steady electrochemical window between 0 and 5 V[33], with no other peaks observed in the tested samples[29]. The electrochemical window of the $\text{Na}_3\text{SbP}_{0.16}\text{S}_{3.6}\text{O}_{0.4}$ -500 heat treated at 500 °C, was the most stable, as evidenced by its consistent linear response. This further demonstrated that the electrochemical stability of the P–O structure was crucial for the cycle stability of the solid electrolyte. The typical attenuation of current during the measurement process using the enhanced chronoamperometry method is shown in Fig. 6(c). The electronic conductivity was calculated using the equation: $\sigma_e = \left(\frac{l}{s}\right)\left(\frac{dl_e}{du}\right)$, and its value was determined to be $6.11 \times 10^{-5} \text{ mS cm}^{-1}$. The electronic conductivity was at least five orders of magnitude lower than that of all samples[34], indicating extremely low electron conductivity in the electrolyte. Considering that sodium ions played a prominent role in the ion conduction process, the reduction of electromigration and the maintenance of a high

degree of ion conductivity suggested that the battery was durable and resistant to short circuits[35]. As opposed to electronic conductors, the prepared electrolytes were excellent ionic conductors. One of the main limitations for sulfide solid electrolytes in battery applications is their air sensitivity. Air sensitivity hinders their potential as high-performance batteries. Hard acid and soft base theory suggests that the hard base O in the H₂O molecule reacts with the hard acid P in Na₃PS₄ to form a P–O bond, whereas the soft base S reacts favorably with the hard H to release. However, P and O were combined preferentially to produce a stable bridge oxygen structure in NaSbPSO. Additionally, the SbS₄ group remained stable at ambient temperature and pressure due to strong interaction between the soft acid Sb⁵⁺ and the soft base S²⁻. A cubic phase Na₃SbS₄ was synthesized as a reference material to assess the effect of ion substitution on the electrolyte samples' air stability. The amount of H₂S released by the doped sulfide solid electrolyte with oxygen and P elements was observed in humid air (Fig. 6[d]). Compared with the undoped Na₃SbS₄ electrolyte, the release of H₂S gradually decreased with increasing heat treatment temperature, and the release from Na₃SbP_{0.16}S_{3.6}O_{0.4}-500 within 20 min was only 0.202 cm³ g⁻¹, which was a quarter of that from the pure Na₃SbS₄ electrolyte. This result strongly depended on the electrochemically stable structure formed by oxygen doping and the reduction of sulfur content, which served as the basis for the stability of the electrolyte material.

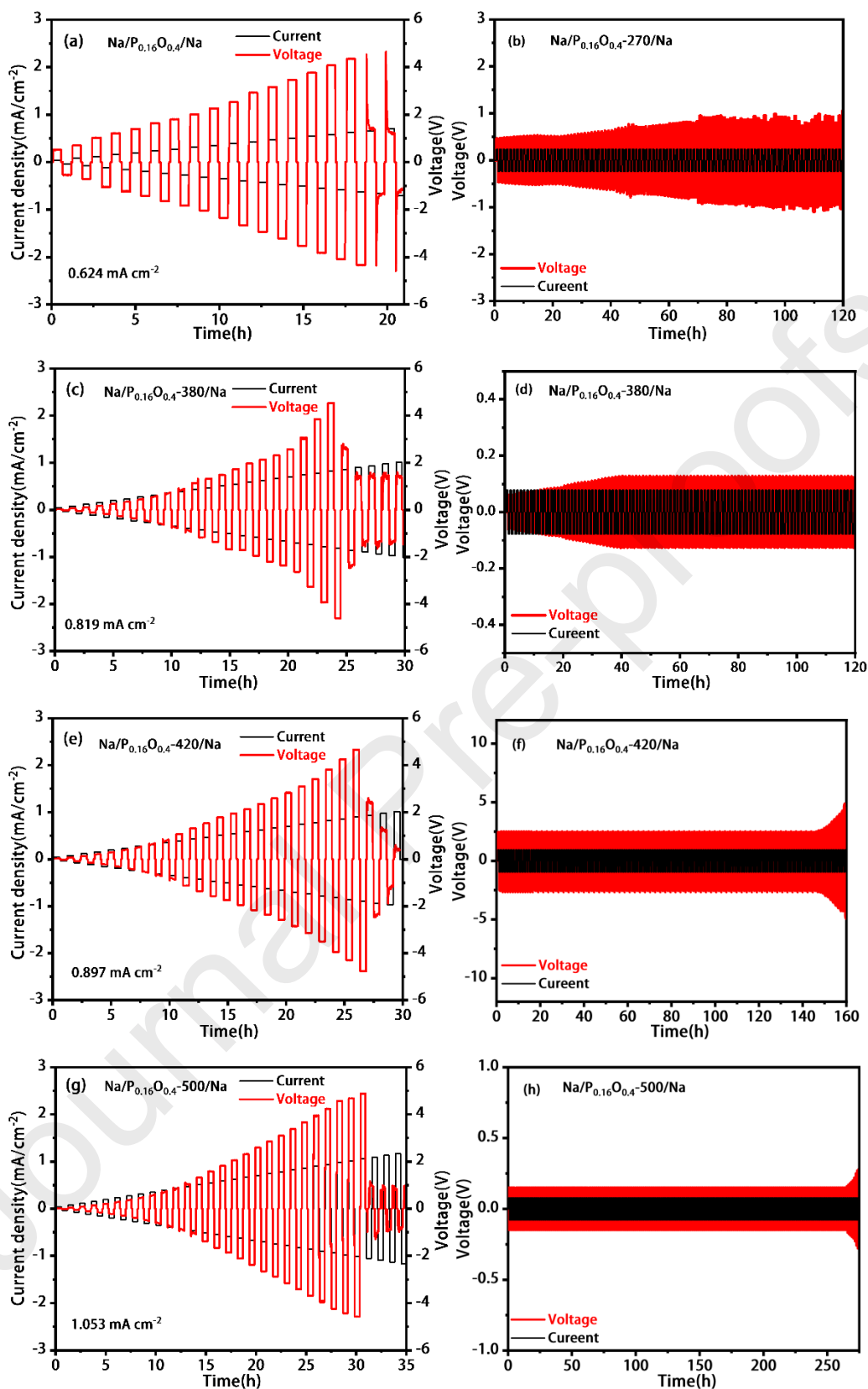


Fig. 8. DC cycling at step-increasing current densities at room temperature of the solid electrolytes $\text{Na}_3\text{SbP}_{0.16}\text{S}_{3.6}\text{O}_{0.4}$ -270(a), $\text{Na}_3\text{SbP}_{0.16}\text{S}_{3.6}\text{O}_{0.4}$ -380(c), $\text{Na}_3\text{SbP}_{0.16}\text{S}_{3.6}\text{O}_{0.4}$ -420(e), and $\text{Na}_3\text{SbP}_{0.16}\text{S}_{3.6}\text{O}_{0.4}$ -500(g). DC cycling tests of $\text{Na}_3\text{SbP}_{0.16}\text{S}_{3.6}\text{O}_{0.4}$ -270(b), $\text{Na}_3\text{SbP}_{0.16}\text{S}_{3.6}\text{O}_{0.4}$ -380(d), $\text{Na}_3\text{SbP}_{0.16}\text{S}_{3.6}\text{O}_{0.4}$ -

420(f), and $\text{Na}_3\text{SbP}_{0.16}\text{S}_{3.6}\text{O}_{0.4}$ -500(h) solid electrolytes at ambient temperature with a current density of 0.1 mA cm^{-2} .

The recyclability of the $\text{Na}_3\text{SbP}_{0.16}\text{S}_{3.6}\text{O}_{0.4}$ electrolyte was investigated in a symmetrical Na | SE | Na battery utilizing gradient current and constant current experiments, as illustrated in Figs. 7(a), (c), (e), and (g). The voltage distribution across the electrolyte exhibited an Ohmic response, $V = IR$. The critical current density (CCD) of these solid electrolytes was defined as the current at which the voltage distribution of the electrolyte suddenly spikes. With increasing temperature, the CCD of $\text{Na}_3\text{SbP}_{0.16}\text{S}_{3.6}\text{O}_{0.4}$ continuously increased[36], reaching a maximum of 1.053 mA cm^{-2} at $\text{Na}_3\text{SbP}_{0.16}\text{S}_{3.6}\text{O}_{0.4}$ -500. In Figs. 7(b), (d), (f), and (h), the electrolytes were subjected to DC cycling tests at room temperature with 0.1 mA cm^{-2} . All four electrolytes exhibited different Ohmic effects, with $\text{Na}_3\text{SbP}_{0.16}\text{S}_{3.6}\text{O}_{0.4}$ -270 and $\text{Na}_3\text{SbP}_{0.16}\text{S}_{3.6}\text{O}_{0.4}$ -380 showing stable voltages of 0.5 V during the 120 h sodium plating/stripping process. The repeated changes in voltage indicated the formation of an unstable interface layer may at the electrolyte interface[37]. As the temperature increased, both $\text{Na}_3\text{SbP}_{0.16}\text{S}_{3.6}\text{O}_{0.4}$ -420 and $\text{Na}_3\text{SbP}_{0.16}\text{S}_{3.6}\text{O}_{0.4}$ -500 exhibited stable sodium electroplating/stripping processes. The initial voltage of $\text{Na}_3\text{SbP}_{0.16}\text{S}_{3.6}\text{O}_{0.4}$ -500 was only 0.2 V, indicating that the transfer impedance of the material was sufficiently minimal to sustain 250 h of stable cycling. The increased bridging oxygen created by the P–O structure considerably improved the interface compatibility between the electrolyte and the sodium anode. The built symmetrical battery displayed good charge discharge cycling properties[38]. The electrolyte clusters were consistently contained and disseminated in the framework, as shown by SEM (Fig. 5). This resulted in consistent sodium metal deposition, efficiently avoided uneven sodium deposition, and reduced the formation of sodium dendrites, all of which contributed to the improved electrochemical stability of the electrolyte material[39].

4. Conclusions

In this work, a novel oxysulfide glass ceramic electrolyte with high ion conductivity and electrochemical stability for sodium metal negative electrodes was successfully synthesized using the high-energy ball milling method and varying heat treatment

temperatures. The electrolyte was systematically tested in a symmetrical battery configuration. The battery, along with Na metal, exhibited excellent electrochemical stability while maintaining ambient temperature ion conductivity of 3.82 mS cm^{-1} . It achieved a CCD of up to 1.053 mA cm^{-2} and stable cycling for up to 260 h in 0.1 mA cm^{-2} . The introduction of P and O elements in the Na_3SbS_4 solid electrolyte led to the formation of oxide and oxygen sulfide units with bridging oxygen characteristics. The homogenization of the glass–ceramic structure was facilitated by the intermediate oxygen sulfide unit, resulting in a decreased electronic conductivity of the electrolyte. Furthermore, the formation of a dynamic stability of self-passivating SEI contributed to excellent electrochemical stability. This research provides a promising strategy for the development of all-solid-state sodium ion batteries with high energy density and long lifespan.

CRedit authorship contribution statement

Lingjun Shu: Methodology, Data curation, Project administration, Writing – original draft. Jingxuan Yin: Investigation. Zhemin Gon: Investigation. Chengwei Gao: Investigation. Xiang Shen: Validation. Yongxing Liu: Validation. Qing Jiao: Writing – review & editing, Funding acquisition, Project administration, Supervision. Other authors have provided suggestions and guidance for the experiment.

Declaration of competing interest

The authors declare that they have no known competing financial interests or personal relationships that could have appeared to influence the work reported in this paper.

Data availability

Data will be made available on request.

Acknowledgements

This work was financially supported by National Natural Science Foundation of China (Grant no. 51972176) and sponsored by K. C. Wong Magna Fund in Ningbo University.

[1] E.R. Cleveland, L.B. Ruppalt, B.R. Bennett, S.M. Prokes, Effect of an in situ hydrogen plasma pre-treatment on the reduction of GaSb native oxides prior to atomic

- layer deposition, *Applied Surface Science*, 277 (2013) 167-175.
- [2] Y. Bai, Y. Zhao, W. Li, L. Meng, Y. Bai, G. Chen, New Insight for Solid Sulfide Electrolytes LSiPSI by Using Si/P/S as the Raw Materials and I Doping, *ACS Sustainable Chemistry & Engineering*, 7 (2019) 12930-12937.
- [3] P. Bron, S. Dehnen, B. Roling, Li₁₀Si_{0.3}Sn_{0.7}P₂S₁₂ – A low-cost and low-grain-boundary-resistance lithium superionic conductor, *Journal of Power Sources*, 329 (2016) 530-535.
- [4] P. Bron, S. Johansson, K. Zick, J. Schmedt auf der Gunne, S. Dehnen, B. Roling, Li₁₀SnP₂S₁₂: an affordable lithium superionic conductor, *J Am Chem Soc*, 135 (2013) 15694-15697.
- [5] A.D. Bui, S.-H. Choi, H. Choi, Y.-J. Lee, C.-H. Doh, J.-W. Park, B.G. Kim, W.-J. Lee, S.-M. Lee, Y.-C. Ha, Origin of the Outstanding Performance of Dual Halide Doped Li₇P₂S₈X (X = I, Br) Solid Electrolytes for All-Solid-State Lithium Batteries, *ACS Applied Energy Materials*, 4 (2021) 1-8.
- [6] H. Cao, M. Yu, L. Zhang, Z. Zhang, X. Yan, P. Li, C. Yu, Stabilizing Na₃SbS₄/Na interface by rational design via Cl doping and aqueous processing, *Journal of Materials Science & Technology*, 70 (2021) 168-175.
- [7] H. Cao, M. Yu, L. Zhang, Z. Zhang, C.J.J.o.M.S. Yu, T. -Shenyang-, Stabilizing Na₃SbS₄/Na interface by rational design via Cl doping and aqueous processing, 70 (2020).
- [8] I.H. Chu, C.S. Kompella, H. Nguyen, Z. Zhu, S. Hy, Z. Deng, Y.S. Meng, S.P. Ong, Room-Temperature All-solid-state Rechargeable Sodium-ion Batteries with a Cl-doped

- Na₃PS₄ Superionic Conductor, Sci Rep, 6 (2016) 33733.
- [9] M. Lazar, S. Kmiec, A. Joyce, S.W. Martin, Investigations into Reactions between Sodium Metal and Na₃PS_{4-x}O_x Solid-State Electrolytes: Enhanced Stability of the Na₃PS₃O Solid-State Electrolyte, ACS Applied Energy Materials, 3 (2020) 11559-11569.
- [10] X. Chi, Y. Zhang, F. Hao, S. Kmiec, H. Dong, R. Xu, K. Zhao, Q. Ai, T. Terlier, L. Wang, L. Zhao, L. Guo, J. Lou, H.L. Xin, S.W. Martin, Y. Yao, An electrochemically stable homogeneous glassy electrolyte formed at room temperature for all-solid-state sodium batteries, Nat Commun, 13 (2022) 2854.
- [11] H. Nguyen, A. Banerjee, X. Wang, D. Tan, E.A. Wu, J.-M. Doux, R. Stephens, G. Verbist, Y.S. Meng, Single-step synthesis of highly conductive Na₃PS₄ solid electrolyte for sodium all solid-state batteries, Journal of Power Sources, 435 (2019).
- [12] N.J.J. de Klerk, M. Wagemaker, Diffusion Mechanism of the Sodium-Ion Solid Electrolyte Na₃PS₄ and Potential Improvements of Halogen Doping, Chemistry of Materials, 28 (2016) 3122-3130.
- [13] D. Escalera - López, K.D. Jensen, N.V. Rees, M. Escudero - Escribano, Electrochemically Decorated Iridium Electrodes with WS_{3-x} Toward Improved Oxygen Evolution Electrocatalyst Stability in Acidic Electrolytes, Advanced Sustainable Systems, 5 (2021).
- [14] H. Gamo, N.H.H. Phuc, R. Matsuda, H. Muto, A. Matsuda, Multiphase Na₃SbS₄ with high ionic conductivity, Materials Today Energy, 13 (2019) 45-49.
- [15] H. Gamo, N.H.H. Phuc, H. Muto, A. Matsuda, Effects of Substituting S with Cl

on the Structural and Electrochemical Characteristics of Na₃SbS₄ Solid Electrolytes, ACS Applied Energy Materials, 4 (2021) 6125-6134.

[16] V. Gulino, L. Barberis, P. Ngene, M. Baricco, P.E. de Jongh, Enhancing Li-Ion Conductivity in LiBH₄-Based Solid Electrolytes by Adding Various Nanosized Oxides, ACS Applied Energy Materials, 3 (2020) 4941-4948.

[17] V. Gulino, M. Brighi, F. Murgia, P. Ngene, P. de Jongh, R. Černý, M. Baricco, Room-Temperature Solid-State Lithium-Ion Battery Using a LiBH₄-MgO Composite Electrolyte, ACS Applied Energy Materials, 4 (2021) 1228-1236.

[18] S. Han, J.Y. Seo, W.B. Park, S.J. Richard Prabakar, S. Park, K.-S. Sohn, M. Pyo, Nominally stoichiometric Na₃(W_xSi_xSb_{1-2x})S₄ as a superionic solid electrolyte, Inorganic Chemistry Frontiers, 9 (2022) 1233-1243.

[19] A. Hayashi, N. Masuzawa, S. Yubuchi, F. Tsuji, C. Hotehama, A. Sakuda, M. Tatsumisago, A sodium-ion sulfide solid electrolyte with unprecedented conductivity at room temperature, Nat Commun, 10 (2019) 5266.

[20] P.M. Shanthi, P.J. Hanumantha, K. Ramalinga, B. Gattu, M.K. Datta, P.N. Kumta, Sulfonic Acid Based Complex Framework Materials (CFM): Nanostructured Polysulfide Immobilization Systems for Rechargeable Lithium-Sulfur Battery, Journal of The Electrochemical Society, 166 (2019) A1827-A1835.

[21] Y. Tian, T. Shi, W.D. Richards, J. Li, J.C. Kim, S.-H. Bo, G. Ceder, Compatibility issues between electrodes and electrolytes in solid-state batteries, Energy & Environmental Science, 10 (2017) 1150-1166.

[22] S. Wenzel, T. Leichtweiss, D.A. Weber, J. Sann, W.G. Zeier, J. Janek, Interfacial

Reactivity Benchmarking of the Sodium Ion Conductors Na₃PS₄ and Sodium beta-Alumina for Protected Sodium Metal Anodes and Sodium All-Solid-State Batteries, ACS Appl Mater Interfaces, 8 (2016) 28216-28224.

[23] B. Ma, Q. Jiao, Y. Zhang, C. Lin, X. Zhang, H. Ma, S. Dai, Structure promoted electrochemical behavior and chemical stability of AgI - doped solid electrolyte in sulfide glass system, Journal of the American Ceramic Society, 103 (2020) 6348-6355.

[24] K.H. Park, D.H. Kim, H. Kwak, S.H. Jung, H.-J. Lee, A. Banerjee, J.H. Lee, Y.S. Jung, Solution-derived glass-ceramic NaI·Na₃SbS₄ superionic conductors for all-solid-state Na-ion batteries, Journal of Materials Chemistry A, 6 (2018) 17192-17200.

[25] H. Muramatsu, A. Hayashi, T. Ohtomo, S. Hama, M.J.S.S.I. Tatsumisago, Structural Change of Li₂S-P₂S₅ Sulfide Solid Electrolytes in the Atmosphere, 182 (2011) 116-119.

[26] W.D. Richards, T. Tsujimura, L.J. Miara, Y. Wang, J.C. Kim, S.P. Ong, I. Uechi, N. Suzuki, G. Ceder, Design and synthesis of the superionic conductor Na₁₀SnP₂S₁₂, Nat Commun, 7 (2016) 11009.

[27] X.H. Rui, Y. Jin, X.Y. Feng, L.C. Zhang, C.H. Chen, A comparative study on the low-temperature performance of LiFePO₄/C and Li₃V₂(PO₄)₃/C cathodes for lithium-ion batteries, Journal of Power Sources, 196 (2011) 2109-2114.

[28] X.H. Rui, N. Yesibolati, S.R. Li, C.C. Yuan, C.H. Chen, Determination of the chemical diffusion coefficient of Li⁺ in intercalation-type Li₃V₂(PO₄)₃ anode material, Solid State Ionics, 187 (2011) 58-63.

[29] H. Wang, Y. Chen, Z.D. Hood, G. Sahu, A.S. Pandian, J.K. Keum, K. An, C. Liang,

An Air-Stable Na₃ SbS₄ Superionic Conductor Prepared by a Rapid and Economic Synthetic Procedure, *Angew Chem Int Ed Engl*, 55 (2016) 8551-8555.

[30] T. Sawabe, M. Akiyoshi, K. Yoshida, T. Yano, Estimation of neutron-irradiation-induced defect in 3C-SiC from change in XRD peak shift and DFT study, *Journal of Nuclear Materials*, 417 (2011) 430-434.

[31] F. Tsuji, N. Masuzawa, A. Sakuda, M. Tatsumisago, A. Hayashi, Preparation and Characterization of Cation-Substituted Na₃SbS₄ Solid Electrolytes, *ACS Applied Energy Materials*, 3 (2020) 11706-11712.

[32] F. Tsuji, A. Nasu, A. Sakuda, M. Tatsumisago, A. Hayashi, Mechanochemical synthesis and characterization of Na₃-P1-W S₄ solid electrolytes, *Journal of Power Sources*, 506 (2021).

[33] H. Wan, J.P. Mwizerwa, F. Han, W. Weng, J. Yang, C. Wang, X. Yao, Grain-boundary-resistance-less Na₃SbS₄-Se solid electrolytes for all-solid-state sodium batteries, *Nano Energy*, 66 (2019).

[34] C. Wei, S. Chen, C. Yu, R. Wang, Q. Luo, S. Chen, Z. Wu, C. Liu, S. Cheng, J. Xie, Achieving high-performance Li_{6.5}Sb_{0.5}Ge_{0.5}S₅I-based all-solid-state lithium batteries, *Applied Materials Today*, 31 (2023).

[35] W. Weng, G. Liu, Y. Li, L. Shen, X. Yao, Tungsten and oxygen co-doped stable tetragonal phase Na₃SbS₄ with ultrahigh ionic conductivity for all-solid-state sodium batteries, *Applied Materials Today*, 27 (2022).

[36] W. Weng, G. Liu, L. Shen, X. Yao, High ionic conductivity and stable phase Na_{11.5}Sn₂Sb_{0.5}Ti_{0.5}S₁₂ for all-solid-state sodium batteries, *Journal of Power*

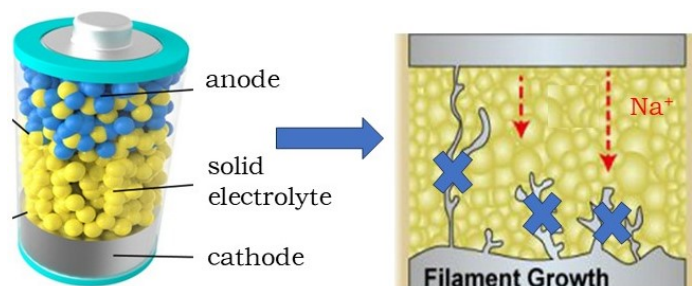
Sources, 512 (2021).

[37] S. Xiong, Z. Liu, L. Yang, Y. Ma, W. Xu, J. Bai, H. Chen, Anion and cation co-doping of Na₄SnS₄ as sodium superionic conductors, Materials Today Physics, 15 (2020).

[38] R. Xu, Z. Wu, S. Zhang, X. Wang, Y. Xia, X. Xia, X. Huang, J. Tu, Construction of All-Solid-State Batteries based on a Sulfur-Graphene Composite and Li_(9.54)Si_(1.74)P_(1.44)S_(11.7)Cl_(0.3) Solid Electrolyte, Chemistry, 23 (2017) 13950-13956.

[39] B. Zhang, L. Yang, L.-W. Wang, F. Pan, Cooperative transport enabling fast Li-ion diffusion in Thio-LISICON Li₁₀Si₂S₁₂ solid electrolyte, Nano Energy, 62 (2019) 844-852.

The co doping of P and O in the Na_3SbS_4 electrolyte system resulted in a uniform bridging oxygen structure, stabilizing the interface between the sodium metal and the electrolyte, and maintaining a constant current cycling at room temperature for 260 h.



Declaration of interest statement

We declare that we have no financial and personal relationships with other people or organizations that can inappropriately influence our work, there is no professional or other personal interest of any nature or kind in any product, service or company that could be construed as influencing the position presented in, or the review of, the manuscript entitled “Enhancing interface stability and ionic conductivity in the designed $\text{Na}_3\text{SbP}_{0.4x}\text{S}_{4-x}\text{O}_x$ sulfide solid electrolyte through bridging oxygen”.

CRedit authorship contribution statement

Lingjun Shu: Methodology, Data curation, Project administration, Writing – original draft. Chengwei Gao: Investigation. Yongxing Liu: Investigation. Xiaolong Zhou: Investigation. Xiang Shen: Validation. Shixun Dai and Changgui Lin: Validation. Qing Jiao: Writing – review & editing, Funding acquisition, Project administration, Supervision. Other authors have provided suggestions and guidance for the experiment.